Journal of The Electrochemical Society, **161** (5) F615-F621 (2014)
0013-4651/2014/161(5)/F615/7/$31.00 © The Electrochemical Society

Influence of Sulfone Linkage on the Stability of Aromatic Quaternary Ammonium Polymers for Alkaline Fuel Cells

Alina Amel,[a] Liang Zhu,[b] Michael Hickner,[b] and Yair Ein-Eli[a,c,*,z]

[a]*Department of Materials Science and Engineering, Technion - Israel Institute of Technology, Haifa 3200003, Israel*
[b]*Department of Materials Science and Engineering, The Pennsylvania State University, University Park, Pennsylvania 16802, USA*
[c]*The Nancy & Stephan Grand Technion Energy Program (GTEP), Technion - Israel Institute of Technology, Haifa 3200003, Israel*

The properties and stability of quaternary ammonium poly(sulfone) QA-RADEL and quaternary ammonium poly(phenylene oxide) QA-PPO were investigated. These two membranes have a major difference in their backbone structure where QA-RADEL contains an electron-withdrawing group and QA-PPO is an ether-based backbone without electron-withdrawing group in the main chain. Conductivity, thickness and swelling measurments were examined at various temperatures for both types of samples. HRSEM and FTIR analysis indicated that QA-RADEL membrane degraded much faster than QA-PPO under high temperature and high pH conditions. QA-RADEL showed degradation at both the cationic groups and the polymer backbone after 150 h at 60°C, while QA-PPO showed degradation merely at the cationic groups after aging for 1000 h at 60°C, under high pH conditions. The sulfone linkage has a profound negative influence on the thermal and alkaline stability of the membrane, which provides design rules for future high-stability AEMs.
 [DOI: 10.1149/2.044405jes]

Manuscript submitted February 10, 2014; revised manuscript received March 11, 2014. Published March 19, 2014.

Currently there is great global demand for clean energy conversion technology and renewable energy systems. Fuel cell research has seen considerable growth in recent years, due to their high energy efficiency and potentially low pollution levels.[1] Among the various kinds of fuel cells, polymer electrolyte fuel cells (PEFCs) incorporating proton exchange membranes have been developed for residential, portable, and electric vehicle applications.[2] Perfluorinated membranes such as Nafion (DuPont) are state-of-the-art proton-conducting membranes for PEFCs. Although these membranes exhibit excellent chemical, mechanical, and thermal stability along with high proton conductivity, there are several obstacles that impede the commercialization of these fuel cells. Among them, their high cost as well as the need for platinum group metal catalysts, and insufficient durability of these materials under fuel cell operating conditions. One possible solution to overcome these problems would be the use of an anion exchange membrane (AEM) that facilitates high pH operation of electrochemical devices. Alkaline fuel cells using AEM have several advantages over proton exchange membrane fuel cells on both cost and performance.[3] The basic environment of alkaline fuel cells offers important benefits, such as enhanced kinetics for oxygen reduction reaction, and reduced corrosion. These factors lead to an increase in fuel cell efficiency and also permit the use of non-noble metal catalysts, making this technology beneficial as a low-cost replacement for the more-common proton exchange fuel cell technology.[4]

Alkaline membrane fuel cells (AMFCs) received a significant attention in recent years.[5] However, there are a few challenges ahead, mainly regarding membranes' chemical stability in the harsh alkaline environment.[6–8] Their chemical stability has been considered mainly in the context of the cationic stability, and the main degradation pathways for ammonium cationic groups in high pH conditions were found to be Hoffman elimination (where possible with β-hydrogens), nucleophilic substitution at the α-carbons on the tether or cation ligands, and ylide intermediate formation.[9,10] In addition to cationic stability, chemical stability of the AEM backbone is another essential and relevant issue and plays a significant role in high stability AEMFCs. For example, the polymer backbone decomposition of polyvinylidene fluoride (PVDF) occurs at high pH, and the mechanism of dehydrofluorination is well-described in the literature,[11] while degradation of polyimides in an alkaline environment occurs when hydroxide ions attack the imide group to eventually form poly(amic acid).[12]

However, there is very little information on the high pH stability of aromatic-based backbones, being presented as aromatic poly(arylene ether)s. This knowledge is especially needed for hydrophilic polymers, where an intimate contact between the polymer chain and the reactive species exist. Fujimoto et al.[13] reported on the backbone stability of benzyltrimethyl ammonium functionalized poly(arylene ether) (PAE) and poly(phenylene) (PP). Their measurements indicated that there is a cleavage of aryl-ether linkage in quaternized PAEs under high pH conditions at 80°C, while no backbone degradation in quaternized PP was observed under the same conditions. Ramani et al.[14] used a 2D NMR technique to investigate the stability of quaternized bisphenol A polysulfone. Using two-dimensional correlated (COZY) H^1 NMR, they demonstrated that the cationic group triggers degradation of the polymer backbone in alkaline environments *via* quaternary carbon hydrolysis and ether hydrolysis, leading to accelerated deterioration. Hickner et al.[15] claimed through polymer fragment modeling that polysulfone's structure adopts a conformation that places the quaternary nitrogen and the electron-rich sulfone's oxygen in close proximity that partially exposes the CH_2–$N(CH_3)_3$ bond, leading to its susceptibility to nucleophilic attack. Additionally, severe molecular weight degradation (measured by an intrinsic viscosity decrease) of a poly(ketone)-based backbone (which would have similar electron-withdrawing properties as a poly(sulfone)-based backbone) was observed.[16]

The main goal of this study is to understand the influence of sulfone linkage on the membranes' stability. We think that the best approach to predict the design of the most stable and highly efficient membrane will comprise of analyzing each and individual component of the membrane and its impact on its properties and stability. This research focus on investigating the influence of the sulfone group in the membrane backbone structure on the degradation behavior of two quaternary ammonium (QA) poly(aromatic) anion exchange polymers: poly(sulfone) (QA-RADEL) and poly(phenylene oxide) (QA-PPO). Since QA-PPO membrane contains no sulfone linkage, it serves in this study as a comparison material to the QA-RADEL membrane. The influence of the sulfone group on the conductivity, swelling, thickness, surface morphology and stability subsequent to high pH exposure is discussed in details.

Experimental

Polymer synthesis.— Two anion exchange membranes were synthesized at Penn State University. Scheme 1(a) shows the chemical structure of a biphenol-based poly(sulfone)-based anion exchange membrane that was synthesized by chloromethylation of a commercially available Radel polymer (QA-RADEL).

*Electrochemical Society Active Member.
[z]E-mail: eineli@tx.technion.ac.il

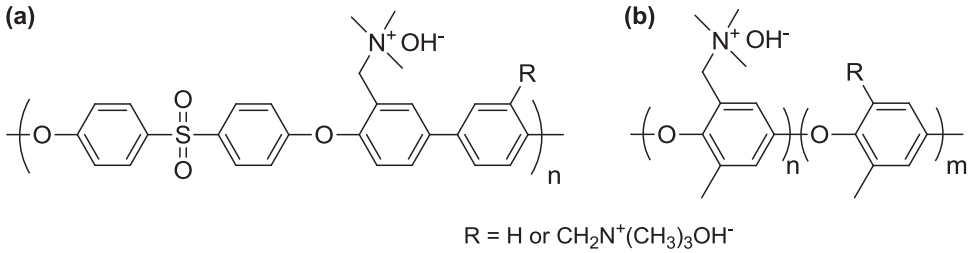

Scheme 1. Chemical structures of (a) quaternary ammonium functionalized poly(sulfone) (QA-RADEL) anion exchange polymer and (b) quaternary ammonium functionalized poly(phenylene oxide) (QA-PPO) anion exchange polymer.

The second membrane was synthesized through quaternary ammonium functionalized poly(phenylene oxide) polymer (QA-PPO) shown in Scheme 1(b) prepared by bromination and quaternization with trimethyl amine. The ion exchange capacities of QA-RADEL and QA-PPO membranes were 2.10 meq g^{-1} and 1.95 meq g^{-1}, respectively.

Characterization.—Water uptake.— The water uptake of HCO_3^- form membranes, was defined as weight ratio of the absorbed water to that of the dry membrane as given by:

$$W(\%) = \left(\frac{m_W - m_D}{m_D}\right) \cdot 100$$

where, m_D and m_W are the mass of the membrane, before and after water absorption, respectively. The membranes were fully immersed in water and periodically weighed on an analytical balance until a constant mass was obtained, giving the mass-based water uptake. Both membranes achieved equilibrium after 30–40 minutes. The procedure of weighing wet membranes includes surface water elimination by rapid surface drying with a Kimwipe paper followed by drying in a vacuum oven for 24 h at a temperature of 60°C.

Thickness increase under hydration.—Thickness increase/decrease of HCO_3^- form membranes, was defined as thickness ratio of the absorbed water membrane to that of the dry membrane, as given by:

$$T(\%) = \left(\frac{t_W - t_D}{t_D}\right) \cdot 100$$

where t_D and t_W are the thicknesses of the membranes, before and after water absorption, respectively. The procedure of measuring membrane thickness follow the exact procedure as described in the previous section.

Ion Exchange Capacity (IEC).—The IECs of the membranes were calculated from the ^{1}H NMR and confirmed by titration. In the ^{1}H NMR method, the degree of functionalization of the quaternary ammonium groups was calculated from the integral ratio of the methylene peak to the polymer backbone peaks, while for the titration method, 0.2 g of membrane was immersed in 50 mL of 0.2 M $NaNO_3$ solution for 24 h and titrated with 0.1 M $AgNO_3$ using K_2CrO_4 as an indicator. The IEC was calculated as follows:

$$IEC = \frac{\Delta V_{AgNO_3} C_{AgNO_3}}{m_d}$$

Where, m_d is the mass of the dry membrane, ΔV_{AgNO3} is the consumed volume of $AgNO_3$ solution and C_{AgNO3} is the concentration of $AgNO_3$ solution.

High Resolution Scanning Microscopy (HRSEM).—HRSEM analysis was carried out using a Zeiss Ultra-Plus FEG-SEM. Membrane samples were cut into squares of approximately 5 × 5 mm^2 and fixed to an aluminum stub with double sided conductive tape, followed by carbon sputter coating. The observation was conducted with an acceleration voltage of 3 kV.

ATR FTIR.—Attenuated Total Reflection Fourier Transform Infra-Red (ATR-FTIR) spectra of the membranes were obtained with the use of a Nicolet spectrometer equipped with a DTGS detector. A reflection ATR accessory equipped with a diamond crystal at an incident angle of 45° was used. The membrane sample was pressed to the crystal by the clamp-kit to ensure reproducible contact between the sample and the ATR crystal.

Ionic conductivity.—The ionic conductivity (σ, S cm^{-1}) of HCO_3^- form membranes (size: 1 cm × 2 cm) was measured by two probe in-plane impedance spectroscopy using $\sigma = d/L_s W_s R$ (d is the distance between reference electrodes, L_s and W_s are the thickness and width of the membrane, respectively). The membrane impedance was measured over the frequency range from 10 kHz to 10 mHz by impedance spectroscopy (EIS) using an PARSTAT 2273 (Princton Applied Research). The resistance of the membranes was determined from the real part of the impedance at the minimum imaginary value. The measurements were under fully hydrated conditions, with the sample membranes being immersed in liquid water. Temperature dependent measurements were performed at a desired temperature after stabilizing the samples for at least 3 h in the targeted temperature.

Results and Discussion

Chemical structure analysis.— Chemical structures of the polymers were investigated by FTIR and the absorption spectra of the membranes are shown in Figure 1. QA-RADEL membrane has a 1200 –1400 cm^{-1} region which is dominated by sulfone[17–19] and ether. Vibrations at 1240 cm^{-1} was assigned to the asymmetric vibration of the ether linkage.[20,21] The enlarged region of 1160–1050 cm^{-1}, displays three distinctive peaks at 1146 cm^{-1}, 1103 cm^{-1} and 1071 cm^{-1}, which are attributed to the symmetric vibration of the sulfone peak, asymmetric vibration of the sulfone-aryl linkage and symmetric peak of the sulfone aryl bond, respectively. As can be seen, these peaks appear only in the QA-RADEL membrane, since the QA-PPO membrane lacks the sulfone group. The C_4N^+ vibrations from the quaternary ammonium moieties are centered at 920 cm^{-1}, 955 cm^{-1} and

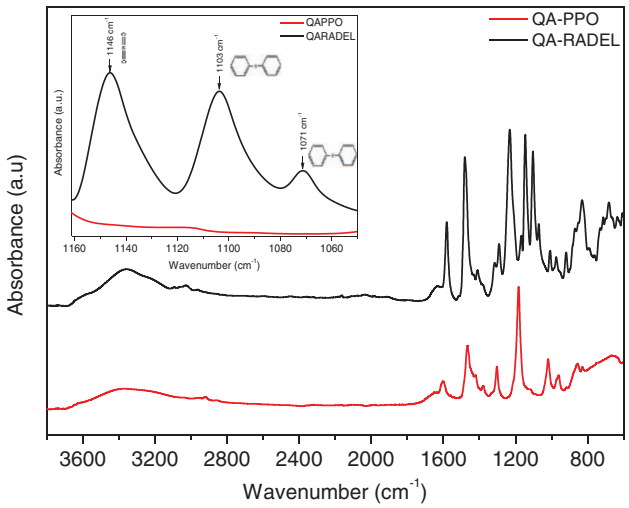

Figure 1. ATR FTIR spectra of QA-RADEL and QA-PPO membranes.

975 cm^{-1}.[22,23] The absorption spectrum of QA-PPO has bands in the 1420–1450 cm^{-1} region, which is dominated by C-C aromatic stretching. The characteristic bands at 1305 cm^{-1} and 1120 cm^{-1} are assigned to ether vibration bands. The C_4N^+ vibrations of quaternary ammonium of QA-PPO are centered at 918 cm^{-1}, 960 cm^{-1} and 970 cm^{-1}. This peaks assignment represents the fundamental difference between the membranes, being reflected in the appearance of the sulfone group. In addition, the relative abundance of the chemical groups will assist us to study the stability in alkaline and to perform a quantitative analytical analysis, by measuring the areas of the absorption peaks. The ratio between these peaks areas will reflect changes and modifications in the membranes chemical structure.

Degree of water uptake and swelling.— Water uptake is known to be an important parameter for ion-conducting membranes, since sample's water content has a strong influence on the membrane conductivity and mechanical properties.[24]

Here, we characterized water uptake of the membranes at different temperatures in cyclic thermal sweeps in the HCO_3^- membrane form. Figure 2 shows that water uptake of QA-RADEL and QA-PPO membranes increases with temperature. Water uptake of QA-RADEL membrane at 25°C is greater, compared to that of QA-PPO sample. As expected, the higher ion exchange capacity (IEC) QA-RADEL membrane absorbed more water than the QA-PPO sample, due to their increased ion content. As shown in Figure 2, water uptake of QA-RADEL membrane increased from 40 wt% at room temperature to 70 wt% at 60°C, while the water uptake by QA-PPO increased from 20 wt% at room temperature to 30 wt% at 60°C. In addition, QA-RADEL showed significant temperature hysteresis, and irreversibly swelled upon warming in liquid water. Some irreversible swelling of the QA-PPO sample was observed as well, however it was in a much lower extent. The polar nature of the RADEL backbone and its initially larger water uptake may cause it to swell to a much larger extent upon heating than QA-PPO.

Thickness increase measurments with temperature (Figure 3) showed the same trends as the gravimetric water uptake measurements. The membranes' thickness increased as a function of temperature, between 25°C and 60°C. QA-RADEL experienced a significant increase in its thickness, from 5% at room temperature to 23% at 60°C, while the QA-PPO membrane's thickness increase from 3% at 25°C to 7% at 60°C. Both membranes showed some temperature hysteresis and QA-RADEL membrane swelling was much more than the QA-PPO sample, similar to the water uptake measurements.

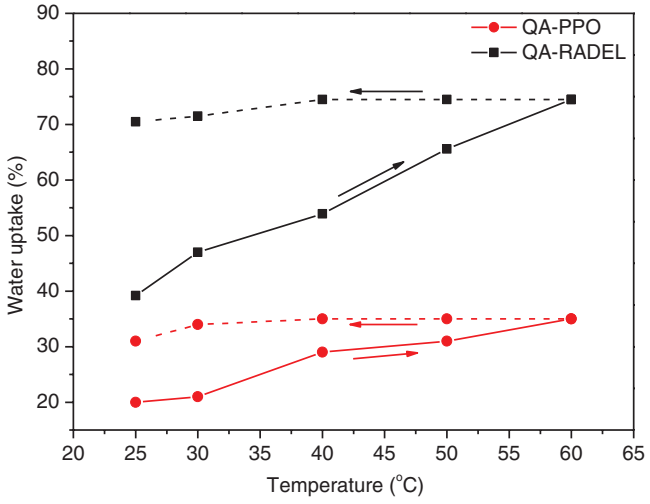

Figure 2. Membranes water uptake as a function of temperature. Temperature was applied in a cyclic manner, from 25 to 60°C and back.

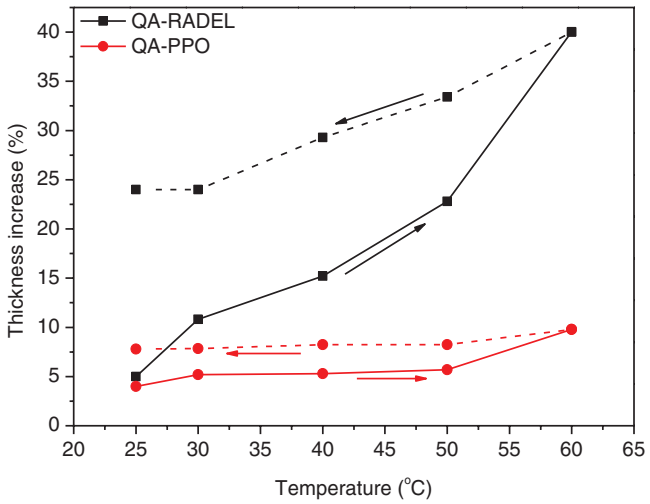

Figure 3. Membranes thickness vs. temperature. Temperature was applied in a cyclic manner from 25 to 60°C and back.

Ionic conductivity.— The ionic conductivity of the membranes in the bicarbonate form as a function of temperature is shown in Figure 4. The ionic conductivities of these membranes increased with temperature. The conductivity of QA-PPO was found to be 3 mS cm^{-1} at room temperature and increased to 8 mS cm^{-1} at 60°C. QA-RADEL conductivity was found to be 9 mS cm^{-1} at room temperature, and increased to 27 mS cm^{-1} at 60°C. The conductivity of QA-RADEL membrane increased to larger values than the QA-PPO sample, due to its larger water uptake ability. Since the ion-conductivity is influenced by polar groups, we assume that the sulfone groups in the QA-RADEL membrane caused the membrane to be more polar and therefore, facilitate more water uptake to promote greater conductivity.

Thermal stability.— The thermal stability of the HCO_3^- form membranes was analyzed using TGA (Figure 5). The temperature was increased from room temperature to 80°C at a heating rate of 10°C min^{-1}. The temperature was held for 30 min to remove most of the residual water from the membrane, and then it was increased to 500°C at a heating rate of 2°C min^{-1}.

Thermal stability of a polymer is an important consideration in the development of membranes for a fuel cell application. Since fuel

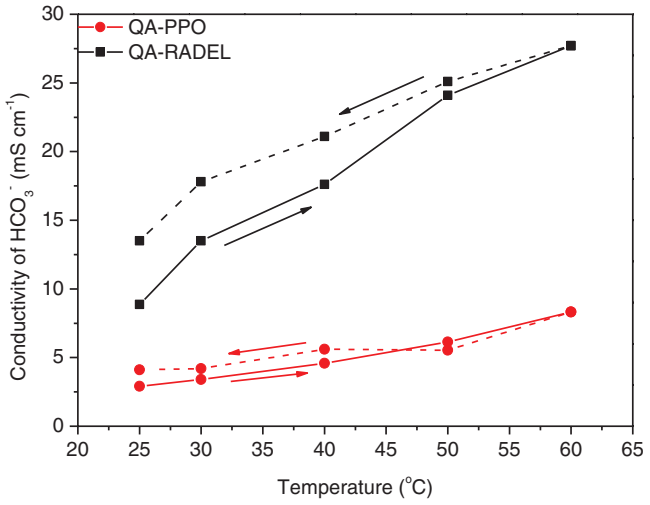

Figure 4. Conductivity of HCO_3^- form of QA-RADEL and QA-PPO membranes vs. temperature. Temperature was applied in a cyclic manner from 25 to 60°C and back.

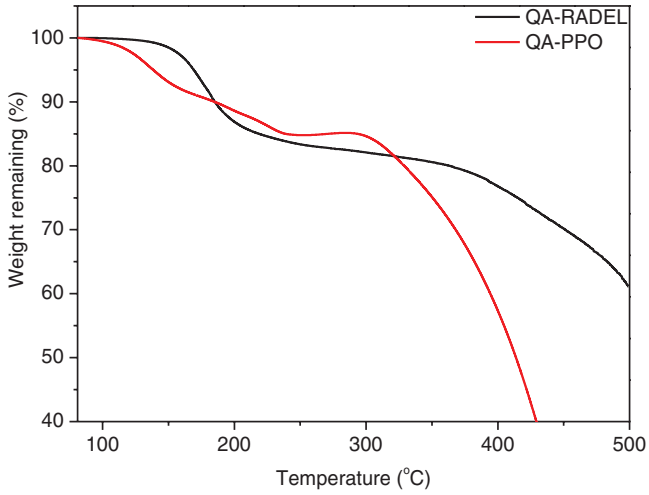

Figure 5. TGA curves of HCO_3^- form of QA-PPO and QA-RADEL membranes.

cells require hydrated stability and thermal breakdown is not as likely during device operation as other forms of chemical and mechanical degradation, importantly, TGA can be used to determine the conditions for hot-pressing of the membrane electrode assembly (MEA) to avoid damage or degradation of the membrane during lamination or hot pressing. Two significant decomposition events were observed, which were ascribed to the decomposition of cationic groups in the first step and the decomposition of the polymer backbone in the second step.[25–29] The first degradation step for the QA-RADEL membrane from 170 to 180°C was attributed to a loss of quaternary ammonium and HCO_3^- ion. We assume that the decomposition temperatures were very close to each other therefore it is quite difficult to distinguish between them. The second significant decomposition step, beginning at 370°C, corresponded to the degradation of the QA-RADEL backbone. TGA for QA-PPO membrane presents three decomposition events; the first one is between 100°C to 150°C, which is attributed to the decomposition of HCO_3^- ion. The second significant decomposition step between 210–260°C is attributed to the loss of quaternary ammonium groups, while the third decomposition step, beginning at 320°C attributed to the main chain. These results show that quaternary ammonium groups are less thermally stable when they are grafted on QA-RADEL membrane backbone with the sulfone groups. We assume that the presence of the sulfone group in QA-RADEL is causing deleterious stability to the quaternary ammonium group. Similar comparative experiments between AEMs with electron withdrawing groups in the backbone, such as poly(sulfone) or poly(ketone), and AEMs with neutral or electron rich backbones, such as poly(styrene) or poly(phenylene oxide) will help to further highlight the role of backbone composition on AEM stability.

Alkaline stability.—FTIR.—Chemical changes and modifications in the membranes during alkaline stability tests were investigated by FTIR (Figures 6 and 7). In order to track changes in the quaternary ammonium and diaryl ether groups, two main peaks were selected. In the QA-RADEL sample (Figure 6), the 920 cm^{-1} and 1240 cm^{-1} peaks were chosen. These peaks are assigned to the C_4N^+ vibration of the quaternary ammonium group and the aryl-oxygen-aryl (diaryl ether) asymmetric vibration, respectively. The peak at 1106 cm^{-1} that was assigned to the asymmetric vibration of sulfone linkage, showed stability during the entire experiment, therefore was used to normalize the spectra. Regarding the QA-PPO membrane (Figure 8), bands at 918 cm^{-1} and 1118 cm^{-1} were investigated. These peaks are attributed to the C_4N^+ vibrations of quaternary ammonium and the aryl-oxygen-aryl asymmetric vibration, respectively. The peak at 1423 cm^{-1} that was assigned to the aromatic C-C stretching bond, was consistent and stable during the experiment, thus was used to normalize the curves.

The relative abundance of chemical groups can be quantified from the areas of the FTIR absorption peaks. The ratio between these areas will reflect changes and modifications in the chemical structure of the (degraded) membranes. The membranes were degraded until the point where they became mechanically unstable and broke into small pieces that could not be recovered. Alkaline stability of these AEMs was investigated under various pH conditions at room temperature and at 60°C. It can be seen in Figure 6a that the intensity of the quaternary ammonium (QA) band at 920 cm^{-1}, corresponding to the C_4N^+ stretch of QA-RADEL membrane at room temperature decreases over time at the 10M solution, while in 1M and 5M solutions almost no decrease was observed. On the other hand, it can be seen in Figure 6b that at 60°C a higher pH leads to faster degradation rates. The degradation of the QA group is well known in the literature and is being explained by S_N2 nucleophilic substitution at the benzyl position or abstraction of the methyl groups from the quaternary ammonium center. Regarding the backbone stability, degradation at the aryl ether group was observed at room temperature (Figure 7a) and at 60°C (Figure 7b) for the QA-RADEL membrane. Obviously both, the quaternary ammonium and the ether linkage are decomposed in thermal and alkaline environment over time.

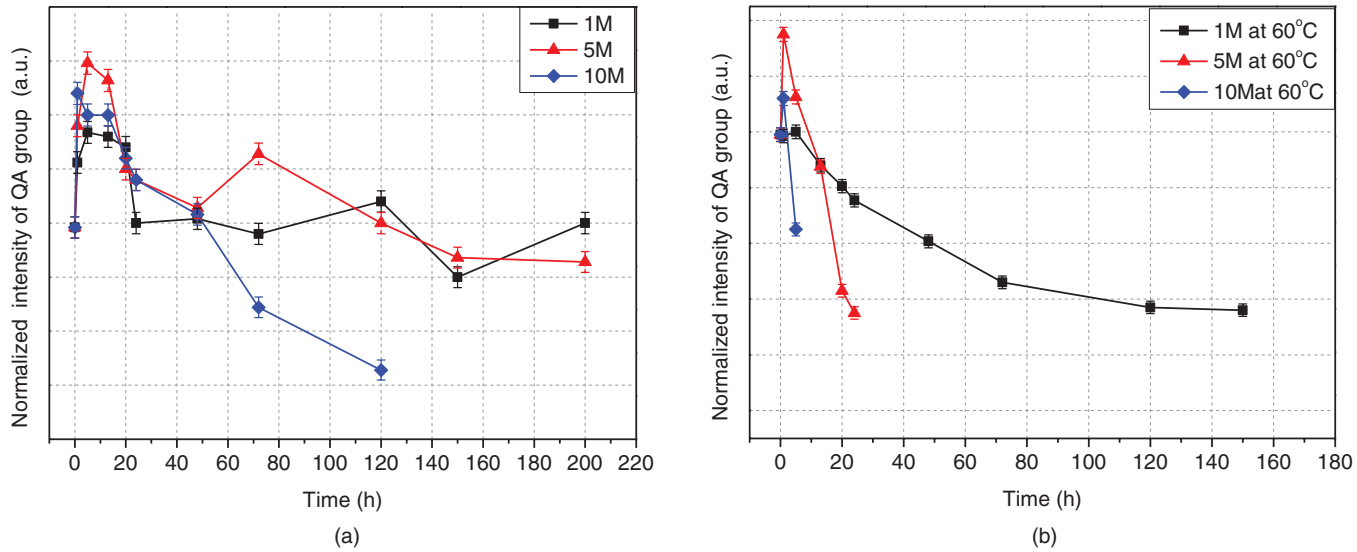

Figure 6. Normalized IR intensity of quaternary ammonium (QA) group in QA-RADEL membrane at room temperature (a) and at 60°C (b).

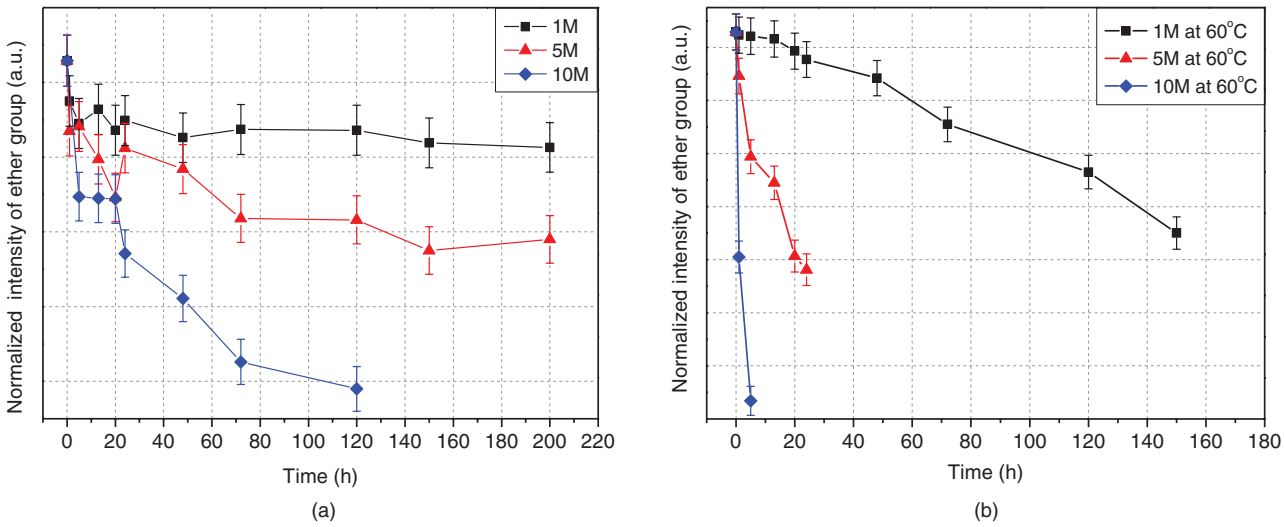

Figure 7. Normalized IR intensity of ether group in QA-RADEL membrane at room temperature (a) and at 60°C (b).

The QA-PPO membrane exhibited QA degradation at high temperature (60°C) and at high pH environment (1–10 M KOH), as can be seen in Figure 8b. At 60°C and 1M KOH conditions after 1000 h, a significant decrease in QA intensity was observed. This degradation rate can be considered a relatively fast for this mild conditions. Higher pH leads to a faster degradation, similar to QA-RADEL membrane (Figure 6b). On the backbone stability issue: our measurements did not detect ether group decomposition under these thermal and alkaline conditions for the QA-PPO sample (Figure 8a).

Comparing this datum with the results reported in the literature will be a bit complicated, since most of the experiments reported were carried out under different conditions and used different characterization technique. For instance, Hibbs et al.[30] observed no change in the IEC values of quaternary ammonium cationic groups based on poly(phenylene) (PP) backbone immersed in 4 M NaOH at 60°C for 28 days. Arges et al.[31] reported on the stability of quaternary ammonium based on polysulfone AEMs stored in 1 and 6 M KOH at 60°C. ^{1}H NMR spectroscopy showed that 90% of the cationic sites remained after 7 days storage at 1 M KOH solution, while only 87% remained subsequent to storage in a 6 M KOH solution. In addition, the relative loss of the ionic conductivity after immersion in 1 M KOH 60°C for 1 day was 37%, while that of 6 M KOH 60°C was 44%. Fujimoto et al.[13] reported on the chemical stability of benzyl trymethyl ammonium cationic groups functionalized on fluorinated and non-fluorinated poly(arylene ether) sulfone and aromatic PP membranes. They did not observed significant change in the cationic groups after immersion in 0.1–0.5 M NaOH at room temperature after 1 h. However, noticeable changes were apparent after storage in 0.5 M NaOH at 80°C for 100 h. Deavin et al.[32] reported on the chemical stability of benzylimidazolium and benzyltrimethylammonium cationic groups using Raman spectroscopy. They reported that imidazolium group is less stable than the benzyltrimethylammonium group in 1 M KOH after 23 days at 60°C. Lin et al.[33] reported that the chemical stability of AEMs with imidazolium cationic groups, [according to ionic conductivity and FTIR measurements] did not changed after 400 h immersion in 1 M KOH at 60°C.

Very few backbone stability experiments were reported. Fujimoto et al.[13] reported on the backbone stability of benzyltrimethyl ammonium functionalized on poly(arylene ether) (PAE) and PP. Their measurements (using FTIR spectroscopy) indicated that there is a cleavage of aryl-ether linkage in quaternized PAEs in 0.5 M NaOH at room temperature and at 80°C after 1 h of immersion. No backbone degradation in quaternized PP was observed under the same conditions. Ramani et al.[14] used 2D NMR technique to report on quaternary carbon and ether hydrolysis of polysulfone expose to 1 and 6 M KOH at 60°C after 30 days. Interestingly, quaternary carbon showed a significant degradation for AEMs samples exposed to 1 M KOH and slow degradation for samples exposed to 6 M KOH

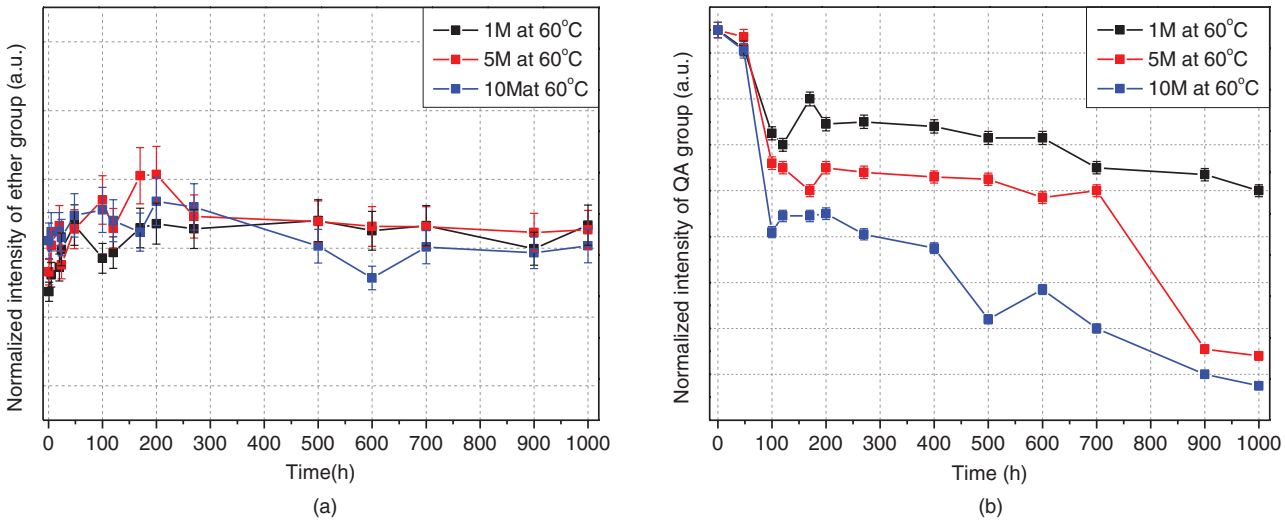

Figure 8. Normalized intensity of ether group (a) and QA group (b) in QA-PPO membrane at 60°C

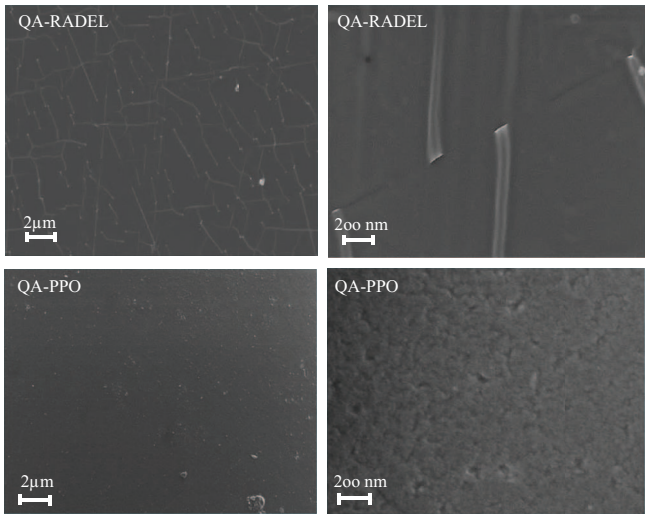

Figure 9. HRSEM images of QA-PPO and QA-RADEL.

solution. On the other hand, ether hydrolysis showed negligible hydrolysis when exposed to 1 M KOH and greater degradation rate in the samples exposed to 6 M solution. They assumed that quaternary carbon hydrolysis required water in one of the intermediate reaction steps for the degradation mechanism to proceed.

Summarizing this part of our results, we can conclude that under alkaline environment QA-RADEL experienced significant changes in the side groups and the polymer backbone structure, while the QA-PPO membrane showed much higher stability under such thermal and alkaline conditions. In other words, the sulfone group in the QA-RADEL backbone had a significant influence on both the QA and the backbone stability of the membrane.

HRSEM analysis.—The surface morphologies of the membranes are presented in Figure 9. The surface of the QA-RADEL sample before degradation was found to be qualitatively different from that of the QA-PPO membrane. QA-RADEL membrane's surface was smooth in appearance, with some small hairline cracking visible. The QA-PPO membrane displayed a rougher surface with no cracking present in the pristine sample. Surface morphology of the membranes was investigated after degradation as well. Figure 10 shows the appearance of small cracks on the QA-RADEL membrane's surface subsequent to immersion in 1 M KOH solution at 60°C for 100 h.

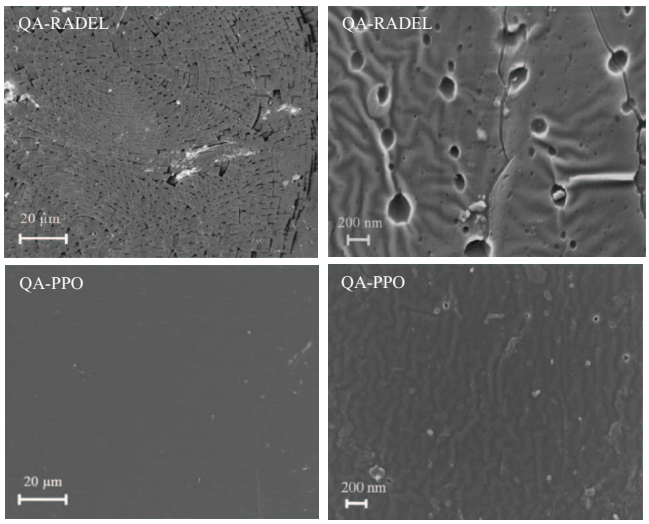

Figure 10. HRSEM images of QA-PPO and QA-RADEL after immersion in 1 M KOH solution at 60°C for 100 h.

Closer inspection revealed the appearance of pits at the surface of the membrane after aging. The cracks and holes are assumed to be due to decomposition of the polymer's backbone that caused some brittleness of the membrane, which eventually break apart disintegrated and/or being dissolved under these aqueous alkaline conditions. The QA-PPO membrane displayed much lower tendency to break apart during aging. Cracks and holes were observed in the QA-PPO membrane; however they were much less pronounced and frequent, as compared to the QA-RADEL membrane.

Conclusions

In conclusion, QA-RADEL membranes showed significant changes in thickness, swelling and conductivity at increasing temperatures as compared to the QA-PPO membrane that swelled to a much lesser extent with increased temperature. Using FTIR spectroscopy, we showed that QA-RADEL's alkaline stability was poor and a severe decomposition *via* the quartenary ammonium and ether group after 150 h at 60°C under a high pH environment occurs. HRSEM revealed that the surface of the membrane suffered from severe cracking showing the presence of pits (holes) as a part of the degradation process. In addition, TGA analysis pointed the low thermal stability of the quartenary groups upon grafting on the QA-RADEL backbone. Unlike QA-RADEL, QA-PPO showed limited physical degradation, as the backbone of QA-PPO was stable and the quartenary ammonium groups decomposed only after 1000 h at 60°C at high pH. These results demonstrate that the sulfone linkage in the polymer backbone has a negative impact on the membrane's backbone and QA group stability in thermal and alkaline conditions. There are two possible ways to deal with this instability, the first one will be to reduce the number of the electron-withdrowing groups from the membrane's backbone, the second will be to synthesize AEMs with long alkyl chains with cations attached at the end of the chain, so they will not be in close proximity to the polymer backbone.

Acknowledgments

This work was supported by the United States-Israel Binational Science Foundation (BSF) through Energy Project No. 2011521 and by the Israel National Research for Electric Propulsion (INREP-ISF grant No. 2797/11) and by the Grand Technion Energy Program (GTEP).

References

1. P. C. Su, C. C. Chao, J. H. Shim, R. Fasching, and F. B. Prinz, *J. Nano Lett.*, **8**, 2289 (2008).
2. B. C. H. Steele and A. Heinzel, *J. Nature*, **414**, 345 (2001).
3. G. Wang, Y. Weng, D. Chu, R. Chen, and D. Xie, *J. Membr. Sci.*, **332**, 63 (2009).
4. J. R. Vorcoe and R. C. T. Slade, *J. Fuel Cells*, **2**, 187 (2005).
5. G. Couture, A. Alaaeddine, F. Boschet, and B. Ameduri, *J. Prog. Polym. Sci.*, **36** 1521 (2011).
6. N. Li, Q. Zhang, C. Wang, Y. M. Lee, and M. D. Guiver, *J. Macromolecules*, **45**, 2411 (2012).
7. F. Zhang, H. Zhang, and C. Qu, *J. Mater. Chem.*, **21**, 12744 (2011).
8. K. A. Page, C. L. Soles, and J. Runt in *Polymers for energy storage and delivery: Polyelectrolytes for batteries and fuel cells*, pp 233–251, ACS Symposium Series Washington, DC (2012).
9. A. C. Cope and E. R. Trumbull in *Olefins from Amines: The Hofmann Elimination Reaction and Amine Oxide Pyrolysis. Organic Reactions*, pp. 317–493, John Wiley & Sons, New York, (2011).
10. S. Chempath, J. M. Boncella, L. R. Pratt, N. Henson, and B. S. Pivovar, *J. Phys. Chem.*, **114**, 11977 (2010).
11. T. N. Danks, R. C. T. Slade, and J. R. Varcoe, *J. Mater. Chem.*, **12**, 3371 (2002).
12. B. Bauer, H. Strathmann, and F. Effenberger, *J. Desalination*, **79**, 125 (1990).
13. C. Fujimoto, D. S. Kim, M. Hibbs, D. Wrobleski, and Y. S. Kim, *J. Membrane Science*, **423-424**, 438 (2012).
14. C. G. Arges and V. Ramani, *J. PNAS*, **110**, 2490 (2013).
15. S. A. Nunñez and M. A. Hickner, *J. ACS Macro Lett.*, **2**, 49 (2013).
16. D. Chen and M. A. Hickner, *J. ACS Applied Materials and Interfaces*, **4**, 5775 (2012).
17. B. Nagel, T. Steiger, J. Fruwert, and G. Geiseler, *J. Spectrochimica Acta*, **31**, 255 (1975).
18. J. H. S. Green, *J. Spectrochimica Acta*, **24**, 1627 (1968).

19. S. Vico, B. Palys, and C. Buess-Herman, *J. Langmuir*, **19**, 3282 (2003).
20. M. Dahlgard and R. Q. Brewster, *J. American Chemical Society*, **80**, 5861 (1958).
21. N. L. Alpert, W. E. Keiser, and H. A. Szymanski, *IR: Theory and practice of infrared spectroscopy*, New York: Plenum Press (1970).
22. R. W. Berg, *J. Spectrochimica Acta*, **34**, 655 (1978).
23. G. Kabisch and G. Möbius, *J. Spectrochimica Acta*, **38**, 1189 (1982).
24. Y. S. Kim, L. Dong, M. A. Hickner, T. E. Glass, V. Webb, and J. E. McGrth, *J. Macromolecules*, **36**, 6281 (2003).
25. M. Tanaka, M. Koike, K. Miyatake, and M. Watanabe, *J. Polym. Chem.*, **2**, 99 (2011).
26. D. Chen, S. Wang, M. Xiao, Y. Meng, and A. S. Hay, *J. Mater. Chem.*, **21**, 12068 (2011).
27. Z. Zhang, L. Wu, J. Varcoe, C. Li, A. L. Ong, S. Poynton, and T. Xu, *J. Mater. Chem. A*, **1**, 2595 (2013).
28. X. Lin, Y. Liu, S. D. Poynton, A. L. Ong, J. R. Varco, L. Wu, Y. Li, X. Liang, Q. Li, and T. Xu, *J. Power Sources*, **233**, 259 (2013).
29. S. D. Poynot, R. C. T. Slade, T. J. Omasta, W. E. Mustain, R. Escudero-Cid, P. Ocon, and J. R. Varcoe, *J. Mater. Chem. A*, in press (2014).
30. M. R. Hibbs, C. H. Fujimoto, and C. J. Cornelius, *J. Macromolecules*, **42**, 8316 (2009).
31. C. G. Arges, J. Parrondo, G. Johnson, A. Nadhan, and V. Ramani, *J. Mater. Chem.*, **22**, 3733 (2012).
32. O. I. Deavin, S. Murphy, A. L. Ong, S. D. Poynton, R. Zeng, H. Hermanac, and J. R. Varcoe, *J. Energy Environ. Sci.*, **5**, 8584 (2012).
33. B. Lin, L. Qiu, B. Qiu, Y. Peng, and F. Yan, *J. Macromolecules*, **44**, 9642 (2011).